

9-1-2021

## The Transport History of Alluvial Fan Sediment Inferred From Multiple Geochronometers

Brent M. Goehring  
*Tulane University*

Nathan Brown  
*University of California, Los Angeles*

Seulgi Moon  
*University of California, Los Angeles*

Kimberly Blisniuk  
*San Jose State University, kimberly.blisniuk@sjsu.edu*

Follow this and additional works at: [https://scholarworks.sjsu.edu/faculty\\_rsca](https://scholarworks.sjsu.edu/faculty_rsca)

---

### Recommended Citation

Brent M. Goehring, Nathan Brown, Seulgi Moon, and Kimberly Blisniuk. "The Transport History of Alluvial Fan Sediment Inferred From Multiple Geochronometers" *Journal of Geophysical Research: Earth Surface* (2021). <https://doi.org/10.1029/2021JF006096>

This Article is brought to you for free and open access by SJSU ScholarWorks. It has been accepted for inclusion in Faculty Research, Scholarly, and Creative Activity by an authorized administrator of SJSU ScholarWorks. For more information, please contact [scholarworks@sjsu.edu](mailto:scholarworks@sjsu.edu).

# JGR Earth Surface

## RESEARCH ARTICLE

10.1029/2021JF006096

### Key Points:

- *In situ* cosmogenic carbon-14 from alluvial fan surfaces can have inheritance regardless of its short half life
- Infrared stimulated luminescence chronology appears to be a robust alluvial fan chronometer
- Geochronometric information can be inverted for sediment history in a catchment upstream of an alluvial fan

### Supporting Information:

Supporting Information may be found in the online version of this article.

### Correspondence to:



B. M. Goehring,  
[bgoehrin@tulane.edu](mailto:bgoehrin@tulane.edu)

### Citation:

Goehring, B. M., Brown, N., Moon, S., & Blisniuk, K. (2021). The transport history of alluvial fan sediment inferred from multiple geochronometers. *Journal of Geophysical Research: Earth Surface*, 126, e2021JF006096. <https://doi.org/10.1029/2021JF006096>

Received 1 FEB 2021  
Accepted 18 AUG 2021

# The Transport History of Alluvial Fan Sediment Inferred From Multiple Geochronometers

Brent M. Goehring<sup>1</sup> , Nathan Brown<sup>2,3</sup>, Seulgi Moon<sup>2</sup> , and Kimberly Blisniuk<sup>4</sup>

<sup>1</sup>Department of Earth and Environmental Sciences, Tulane University, New Orleans, LA, USA, <sup>2</sup>Department of Earth, Planetary, and Space Sciences, University of California-Los Angeles, Los Angeles, CA, USA, <sup>3</sup>Now at University of Texas-Arlington, Arlington, TX, USA, <sup>4</sup>Department of Geology, San Jose State University, San Jose, CA, USA

**Abstract** We present a multi-chronometer approach to refine the age of an alluvial fan and to infer sediment transport and deposition history in the Anza Borrego Desert region of Southern California. We measure *in situ* produced cosmogenic carbon-14 (<sup>14</sup>C) from boulders on the fan surface and infrared stimulated luminescence (IRSL) ages from single feldspar grains within the alluvium. Our new IRSL age [ $5.3 \pm 0.5$  ka ( $\pm 1\sigma$ )] is in excellent agreement with existing uranium-series [U-series;  $5.3 \pm 0.2$  ( $\pm 2\sigma$ )] ages of pedogenic carbonates. The IRSL and U-series ages show that *in situ* <sup>14</sup>C measurements [ $6.6 \pm 1.1$  ka ( $\pm 1\sigma$ )] from boulders contain inherited nuclides from prior exposure in the upstream catchment, much like measurements of the longer-lived nuclide, beryllium-10 (<sup>10</sup>Be). However, *in situ* <sup>14</sup>C ages are closer to the preferred ages inferred from IRSL and U-series and with less scatter than comparative <sup>10</sup>Be ages. Our data demonstrate that a multi-geochronometer approach will produce ages of alluvial fan surfaces with the greatest degree of confidence. We then apply the paired <sup>14</sup>C and <sup>10</sup>Be concentrations to infer the prior exposure and storage duration of the sampled boulders of  $3.1 \pm 3.2$  and  $4.6 \pm 2.3$  Kyr, respectively. A mixture model analysis of the single grain IRSL ages suggests bimodal storage durations prior to remobilization with peaks at ca. 2 and 10 Kyr. We demonstrate that cosmogenic nuclide inheritance and single grain IRSL equivalent dose distributions can provide additional information regarding sediment transport history prior to deposition on the alluvial fan.

**Plain Language Summary** Alluvial fans are the accumulations of sediments stored at the base of mountains. Sediment accumulates via mechanisms that are episodic in nature. Often sediment is stored in the upstream watershed for periods of time before being delivered to the base of the mountain as an alluvial fan, where it is deposited and subsequently buried by younger fan deposits. The ability to date alluvial fan surfaces and subsurface deposits has profound implications for the use of alluvial fans as climate archives and to determine slip rates along faults that offset alluvial fan surfaces. We present measurements of the cosmogenic nuclides carbon-14 and beryllium-10 from boulders from an alluvial fan surface in the Anza Borrego Desert of Southern California, USA, along with measurements of post-infrared infrared luminescence from sands that underlie the same fan surface. Our results show that the luminescence data appear to yield robust ages for sediment accumulation in the fan. The cosmogenic nuclides data is not directly applicable to fan surface age determination. We further show that combining the two geochronometers also yields information about sediment storage in the upstream watershed and that in some cases, sediment can be stored for a longer period of time.

## 1. Introduction

In this article we explore the use of the *in situ* produced cosmogenic nuclides beryllium-10 (<sup>10</sup>Be) and carbon-14 (<sup>14</sup>C) in conjunction with post-infrared infrared stimulated luminescence (p-IR IRSL) measurements from a Holocene alluvial fan in Southern California for both chronometric purposes and to understand sediment storage and mobilization history prior to delivery to alluvial fans. This is important because alluvial fan deposits are recognized as potential archives of past climatic and tectonic activity (e.g., Allen & Densmore, 2000; Brooke et al., 2018; Dorn, 1994; Dühnforth et al., 2017; Frankel et al., 2007; Ritter et al., 1995). However, placing observations related to alluvial fan forms and processes within a Late Pleistocene climatic context requires accurate and precise ages of fan surfaces and deposits (e.g., Owen et al., 2014). Additionally, surface exposure dating has been used in conjunction with offset fan surface features as piercing points for the determination of fault slip rates (e.g., Frankel et al., 2007; Le et al., 2007). Improvement of seismic hazard

assessment models are reliant on robust slip rates that are ultimately limited by chronologic constraints, especially considering improved geomorphic mapping abilities resulting from the advent of high-resolution topography and image datasets. We thus set out to improve upon existing chronometric approaches to date alluvial fan surfaces (Scheuwly-Bollschweiler et al., 2013) largely motivated by the broad questions above.

Efforts to establish absolute chronologies of alluvial fan development have focused on two principal areas, but certainly not limited to: (a) the dating of surface materials almost exclusively via cosmogenic nuclide surface exposure dating (i.e., an exposure event) and (b) the dating of subsurface materials through luminescence, uranium-series, and radiocarbon dating (i.e., a burial event). Here, we briefly review past applications of cosmogenic nuclide and luminescence methods to alluvial fans, including strengths and weaknesses of each as they are the focus of our work. Our review is not meant to be comprehensive, but rather provide background for the methods and results presented in this study.

Studies employing surface exposure dating largely focus on two different sample collection approaches. The first involves collecting individual samples from the surface of boulders or cobbles. The second is the amalgamation of multiple boulders, cobbles, pebbles, granules, and/or sand size material into a single sample (e.g., Anderson et al., 1996; Blisniuk et al., 2012). Amalgamation is also commonly applied in the collection of cosmogenic nuclide depth profiles. Beryllium-10 ( $^{10}\text{Be}$ ), aluminum-26 ( $^{26}\text{Al}$ ), and chlorine-36 ( $^{36}\text{Cl}$ ) are the most commonly measured cosmogenic nuclides; all are radioactive with half-lives of 1.38, 0.705, and 0.301 Myr, respectively. The fact that all of these nuclides are long-lived relative to Holocene alluvial fan surfaces means that they commonly preserve nuclides accumulated during erosion, transport, and storage in the upstream catchment before delivery to the fan surface.

Cosmogenic nuclide inheritance is one of the major limitations in the dating of alluvial fan surfaces using cosmogenic nuclide techniques. The resulting average exposure ages are too old and typically yield a large spread in resulting exposure ages (e.g., discussion in Prush & Oskin, 2020). As surface ages become younger, the relative influence of inheritance becomes more problematic. A similarly skewed age distribution is also observed in landscapes that experience protracted periods of surface aggradation (D'Arcy et al., 2019). Amalgamation techniques aim to improve both accuracy and precision via natural averaging, rather than the averaging of many measurements, but can still be susceptible to inheritance issues (Blisniuk et al., 2012). Finally, cosmogenic nuclide depth profiles have the potential to identify the magnitude of inheritance and the surface age, but they are reliant on uniform inheritance over a range of grain sizes and can be very sensitive to the surface erosion rate (e.g., Anderson et al., 1996; Hidy et al., 2010). Thus, the tendency for surface exposure dating of alluvial fans is to overestimate the age of the fan with poor precision relative to other geochronometers.

The recent development of routine extraction of *in situ* produced cosmogenic  $^{14}\text{C}$  (*in situ*  $^{14}\text{C}$ ) from quartz means it can be applied more broadly in cosmogenic nuclide studies than it has in the past. The short half-life of  $^{14}\text{C}$  (5.73 Kyr) compared to other cosmogenic nuclides means that *in situ*  $^{14}\text{C}$  is potentially less susceptible to inheritance (i.e., less memory of pre-depositional exposure history) and thus has great potential in alluvial fan dating studies. In addition, analyses using multiple nuclides (e.g., *in situ*  $^{14}\text{C}$  and  $^{10}\text{Be}$ ) with their differing half-lives potentially allow for the investigation of sediment transport, storage, and depositional histories (e.g., Fülöp et al., 2020; Hippe, 2017).

Luminescence dating is commonly used to constrain the depositional timing of fluvial deposits (see review by Rittenour, 2008), and especially river and marine terraces (Lewis et al., 2009; Malatesta et al., 2017). Unlike cosmogenic nuclide depth profile techniques, which describe the age of a geomorphic surface that is, susceptible to inheritance and surface erosion, luminescence dating targets the deposition age of a sediment package (Brown, 2020). In other words, a complicated aggradational and erosional history of a terrace can potentially be resolved (Foster et al., 2017). Another advantage of luminescence dating is the ubiquity of datable material, either quartz or K-feldspar grains. Luminescence signals grow on timescales of  $10^2$ – $10^5$  yr and can therefore archive information about active tectonic deformation (Salisbury et al., 2018; Stockmeyer et al., 2017) or recent shifts in climate (Antinao et al., 2016; Brown et al., 2015; Saha et al., 2021).

As alluvial fans are deposited, not all sand grains will be exposed to sunlight long enough for the luminescence signal to completely reset (Colarossi et al., 2015). To overcome this problem, studies have applied single grain dating methods to identify the subset of grains that were completely bleached before deposition,

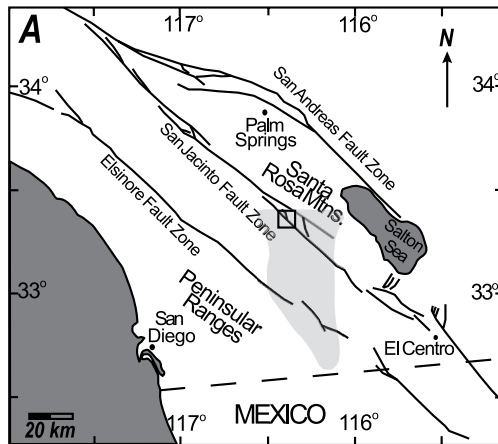


**Figure 1.** Map showing the location of the Anza Borrego Desert, shaded in gray, in Southern California. The square shows the approximate location of Figure 2. Also shown is the San Andreas Fault System, comprising the San Andreas, San Jacinto, and Elsinore fault zones, all of which displace alluvial fans.

that is, the grains that give the true depositional age of a sediment package (Glignani et al., 2017). By measuring the distribution of apparent burial ages within single grain populations of individual samples, researchers can also infer depositional characteristics for a river system (e.g., flood recurrence intervals or average transport distance; Gray et al., 2019; McGuire & Rhodes, 2015).

The advent of widely applicable *in situ*  $^{14}\text{C}$  surface exposure dating and the development of single grain p-IR IRSL techniques motivates the systematic investigation of these two methods for alluvial fan chronology. As such, we selected an alluvial fan in the Anza Borrego Desert region of Southern California, where previous *in situ* produced cosmogenic nuclides  $^{10}\text{Be}$  and U-series dating efforts are available (Blisniuk et al., 2012). We assess the efficacy of *in situ*  $^{14}\text{C}$  and p-IR IRSL dating where results can be benchmarked against existing ages. Below we present measurements of *in situ*  $^{14}\text{C}$  from five boulders previously sampled for  $^{10}\text{Be}$  surface exposure dating and p-IR IRSL ages from four samples from sandy subsurface deposits. Our results show that *in situ*  $^{14}\text{C}$  is not immune to nuclide inheritance, and that p-IR IRSL can provide robust and reliable ages of alluvial fan sediment deposition in arid environments. We also present estimates of the prior exposure and storage duration of boulders delivered to the fan surface through (a) inversion of the measured  $^{14}\text{C}$

and  $^{10}\text{Be}$  concentrations and the deposition ages provided by U-series and p-IR IRSL techniques and (b) single-grain age subpopulations from p-IR IRSL techniques.

## 2. Study Area: The Anza Borrego Desert Region

The study area is located in the northernmost region of the Anza Borrego desert, part of the Sonoran Desert in the western United States (Figure 1). The Anza Borrego desert is bordered by Jurassic metamorphic and Cretaceous plutonic rocks of the Peninsular Ranges in the west, and the Salton Trough in the east (Figure 1; e.g., Axen & Fletcher, 1998; Matti & Morton, 1993; Powell, 1993; Remeika & Lindsay, 1992). The landscape encompasses both lowlands and mountainous regions, with annual precipitation in the desert averaging  $150\text{--}230\text{ mm yr}^{-1}$  in the lowlands and  $380\text{--}530\text{ mm yr}^{-1}$  in the mountainous region (<http://prism.oregon-state.edu>).

The field site, Ash Wash, is located southwest of the San Jacinto fault zone (Figure 1). The Ash Wash alluvial fan deposit dated in this study is located along the southwestern slope of Coyote Mountain in Anza Borrego State Park. This fan is offset by the Coyote Creek Fault strand of the San Jacinto Fault and provides an excellent location to evaluate ages from multiple geochronometers and examine sediment history, because existing geochronologic datasets from U-series and  $^{10}\text{Be}$  exposure dates are available. Blisniuk et al. (2012) collected samples from the top-most surface of boulders within debris flow lobes for cosmogenic nuclide exposure dating on the fan surface and pedogenic carbonate samples for U-series dating from the shallow (0.84–1.3 m) subsurface. In this study we focused on the Q3b alluvial fan identified and dated by Blisniuk et al. (2012) to  $5.2 \pm 0.3\text{ ka}$  ( $\pm 2\sigma$ ) with U-series methods. The Q3b alluvial fan surface exhibits bar and swale relief on the order of 70–100 cm (Blisniuk et al., 2012). The bar surface is characterized by fine-to-coarse grained unweathered quartz diorite and quartz monzonite boulders, characteristic of the upstream bedrock lithologies (Dibblee & Mich, 2008). The bars are leveed by large boulders typically less than 1 m in diameter. Surface morphologic characteristics between the modern active fan and the Q3b alluvial surface suggest the Q3b fan surface is abandoned. The active fan is lower in elevation and inset into the Q3b fan. The Q3b surface consist of slightly smoothed bar and swale topography and has a higher abundance of vegetation further indicates an inactive fan surface (Figure 2). Furthermore, the Q3b fan surface is offset from the modern channel to the due to activity along the Coyote Creek Fault (Figure 2) and therefore has little opportunity to accumulate sediment from the channel.

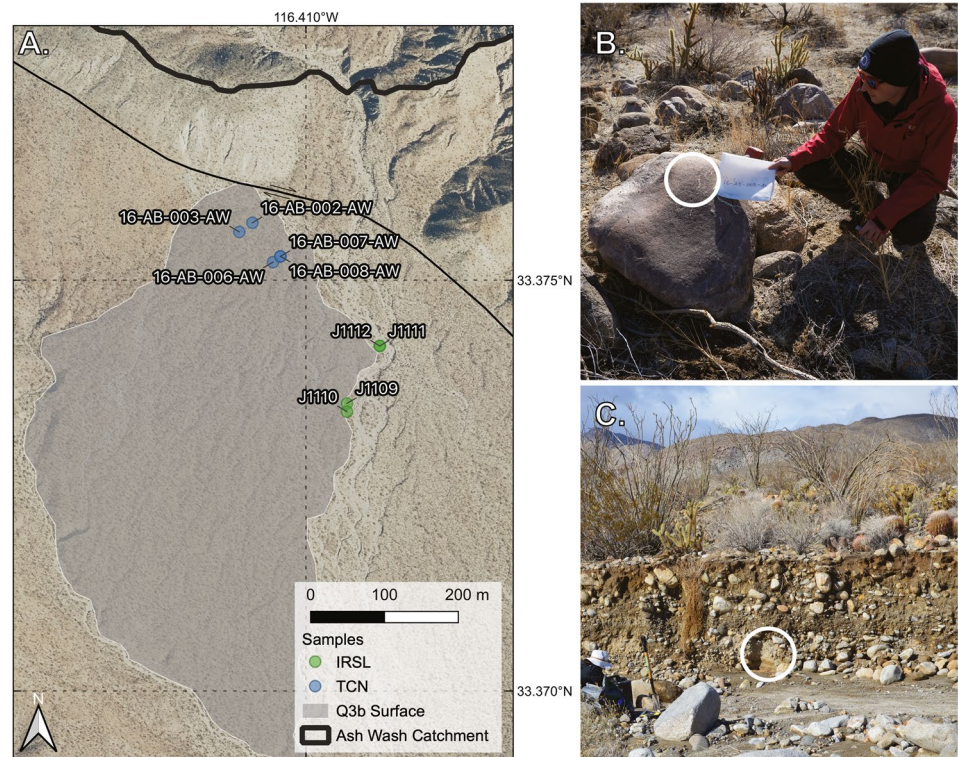


**Figure 2.** Shaded relief map of the Ash Wash catchment (a). Sample locations for cosmogenic nuclide and post-IR IRSL samples. Photos of characteristic samples for cosmogenic nuclide measurements (b) and post-IR IRSL (c) with sampled surfaces or sediment shown by white circles. Note the sub-to well-rounded boulders on the surface and in the sub-surface, the latter are bound within a coarse to medium sand matrix. The Q3b IRSL samples is identified by the white circle within a lens of lighter-colored sands.

### 3. Methods

#### 3.1. Field Sampling

To compare the results from different chronometers, we resampled alluvial fan boulders that comprised some of the amalgamated samples in Blisniuk et al. (2012). Blisniuk et al. (2012) collected material from 9 to 10 boulder surfaces within a debris flow lobe and amalgamated the crushed material to form a single sample; a total of five separate bar surfaces were dated. In the present study, we use a conventional approach to determine if *in situ*  $^{14}\text{C}$  is susceptible to or free of inheritance issues common in  $^{10}\text{Be}$  studies of alluvial fans. We collected five exposure age samples from a single bar surface and kept each sample as an individual sample to examine underlying variability that might be present in the amalgamated measurements of Blisniuk et al. (2012; Figure 2).

The relatively smooth unweathered appearance of the sub-to well-rounded boulders on the Q3b surface (Figure 2b) indicated that sampling with hammer and chisel may be difficult, yet these were the most ideal surfaces for sample collection (e.g., far from edges, topmost boulder surface). We therefore employed a Li-ion battery powered angle-grinder with a dry diamond impregnated blade to collect samples from the optimal sample surface. Sample location was determined using a hand-held GNSS GPS receiver with a typical averaging time of 10 min and net total accuracy of <1 m. Elevation was determined using barometric altimeter calibrated to known elevations daily. Topographic shielding was measured using hand-held sighting inclinometer.

We collected four samples for p-IR IRSL dating from medium-to-coarse sand deposits beneath alluvial fan surfaces (Figure 2c). There was only a single sand lens suitable for luminescence dating, sample J1109, sampled 1.4 m below the Q3b fan surface. Three other samples, J1110 through J1112, were collected from

adjacent inset terraces, at a height about 1 m above the modern channel. These younger terraces lack soil development and range from sandy alluvium to cobble-supported sequences.

### 3.2. Cosmogenic Nuclide Methods

Samples were described in hand sample for lithologic identification, thicknesses measured using calipers, and crushed, milled, and sieved to isolate the 250–710  $\mu\text{m}$  size fraction. Crushed samples were then rinsed in tap water to remove fine mineral coatings and dried. Non-magnetic minerals were isolated using a Carpco-style induced roll magnetic mineral separator, and feldspars removed via froth-flotation (Nichols & Goehring, 2019). All samples then received at a minimum two 5% hydrofluoric acid/5% nitric acid leaches on a room-temperature oscillating shaker table and then two 1% hydrofluoric acid/1% nitric acid leaches in a 50°C ultrasonic bath. Aliquots for  $^{14}\text{C}$  and  $^{10}\text{Be}$  analysis were separated from the pure quartz mineral fractions.

#### 3.2.1. *In Situ* $^{14}\text{C}$

$^{14}\text{C}$  was extracted in the Tulane University Cosmogenic Nuclide Laboratory using the fully automated carbon extraction and graphitization system. Full system and methodological descriptions can be found in Goehring et al. (2019) and are derived from those elsewhere (Goehring et al., 2014; Lifton et al., 2015; Pigati et al., 2010). To briefly summarize, the first day is spent degassing the  $\text{LiBO}_2$  used to fuse the quartz, degassing the alumina combustion boat containing the flux and sample, and finally baking the quartz sleeve used to protect the furnace tube at 1,200°C in a high-purity  $\text{O}_2$  atmosphere. On the second day, the sample is loaded directly onto cooled and solidified  $\text{LiBO}_2$  and reinserted into the tube furnace. The sample is then step-heated first at 500°C for 30 min in an  $\text{O}_2$  atmosphere and then fused and carbon species released at 1,100°C for three hours in an  $\text{O}_2$  atmosphere. The evolved  $\text{CO}_2$  is collected cryogenically and purified before manometric determination of the carbon yield. Samples were diluted to  $\sim 300 \mu\text{g C}$  if the native carbon content was less than 100  $\mu\text{g C}$  via addition of  $^{14}\text{C}$ -free  $\text{CO}_2$ . A small aliquot is then collected in a He over-pressured septum-sealed exetainer for  $\delta^{13}\text{C}$  analysis. The remaining  $\text{CO}_2$  is diverted to a reactor for  $\text{H}_2$  reduction over a Fe catalyst to form graphite, that is, then loaded into cathodes for accelerator mass spectrometry (AMS) analysis.

Process blanks were measured with every eight samples processed using identical procedures to that used for samples, with the exception that no sample was added at the start of the second day. The correction for background  $^{14}\text{C}$ , largely derived from the alumina boat (Goehring et al., 2019), is based on the average of all blanks measured since April 2016 and yields a mean and standard deviation of  $(95.3 \pm 5.94) \times 10^3$  atoms  $^{14}\text{C}$ . Reported  $^{14}\text{C}$  uncertainty is the quadratic combination of (a) the background correction (ca. 25% of the total number of  $^{14}\text{C}$  atoms measured in a sample) and (b) individual sample uncertainty based replicate analyses of an intercomparison quartz material in place of measured uncertainty.

$^{14}\text{C}/\text{carbon-13}$  ( $^{14}\text{C}/^{13}\text{C}$ ) isotope ratios were determined at the Lawrence Livermore National Laboratory Center for AMS. Isotope ratios are determined relative to the NIST Oxalic acid–II primary standard with a  $^{14}\text{C}/^{13}\text{C}$  ratio of  $1.4575 \times 10^{-10}$ . All standards are prepared in the same graphite reactors used for sample preparation and thus our samples are fully internally standardized when analyzed. Stable carbon isotope ratios ( $\delta^{13}\text{C}$ ), necessary for determination of  $^{14}\text{C}$  concentrations, were measured at the University of California–Davis Stable Isotope Facility via isotope ratio mass spectrometry.

#### 3.2.2. $^{10}\text{Be}$

Samples for  $^{10}\text{Be}$  analysis were prepared at Tulane University following established procedures based on those widely in use elsewhere (Ditchburn & Whitehead, 1994). Be-carrier was added and is derived from deeply mined phenacite crystals and typically yields long-term  $^{10}\text{Be}/^9\text{Be}$  ratios of  $(1.73 \pm 1.84) \times 10^{-15}$ . Samples were dissolved in 5 ml of concentrated hydrofluoric acid and 1 ml of concentrated nitric acid for every gram of quartz. Dissolved samples were fumed multiple times in hydrochloric acid to remove silica and decompose fluorides, passed through anion columns principally for the removal of Fe, and finally passed through cation columns for the separation of Be from other cations. Resulting Be eluants are precipitated as hydroxide gels, rinsed five times with Milli-Q  $\text{H}_2\text{O}$  adjusted to a pH of 8 to remove boron, and finally dissolved in 8N nitric acid for quantitative transfer to quartz vials for calcination to BeO. The BeO is then

loaded into cathodes for AMS analysis via mixing with niobium powder. A full procedural blank is prepared alongside the batch of samples and is used to correct for background  $^{10}\text{Be}$ . For all samples, background corrections are <2% of the total  $^{10}\text{Be}$  atoms measured. Beryllium isotope ratios were measured at the Purdue Rare Isotope Measurement Laboratory relative to standards prepared by Nishiizumi et al. (2007), with an accepted  $^{10}\text{Be}/^9\text{Be}$  ratio of  $(2.851 \pm 0.0031) \times 10^{-12}$ .

### 3.2.3. Exposure Age Calculation

Exposure ages are calculated using the scaling method for neutrons and protons outlined in Lifton et al. (2014), and a simplified muon scheme presented in Balco (2017), all of which are modulated by the geomagnetic model of Lifton (2016). Reference  $^{10}\text{Be}$  production rates were determined using the CRONUS-Earth “primary” calibration dataset (Borchers et al., 2016). For  $^{14}\text{C}$  production rates, we used the same production rate scaling method as that used for  $^{10}\text{Be}$ . The production rate is calculated assuming that the CRONUS-A interlaboratory comparison standard (Jull et al., 2015) is at steady-state equilibrium and is therefore an ideal production rate calibration sample. Reported  $^{10}\text{Be}$  uncertainties are at the  $1\sigma$  level and include full propagation of analytical errors (quartz mass, carbon mass, AMS uncertainty, and blank uncertainty); typical total analytical error for Tulane-PRIME Lab measurements approximates the scatter reported for  $^{10}\text{Be}$  measured in CRONUS-A (Goehring et al., 2019; Jull et al., 2015). Reported  $^{14}\text{C}$  uncertainties are at the  $1\sigma$  level and either represent the larger of standard deviation for individual sample measurements or scatter derived from replicate measurements (5.6%) of an intercomparison material (Jull et al., 2015; CRONUS-A).

## 3.3. IRSL Methods

### 3.3.1. Environmental Dose-Rate Determination

The total environmental dose rate for each sample was calculated from elemental concentrations of U, Th, K, and *in situ* gamma dose-rate. The *in situ* gamma dose-rate was measured with a calibrated EG&G ORTEC MicroNOMAD portable NaI gamma spectrometer. For sample J1109 this measurement could not be performed because the probe would not fit between cobbles within the sampled sediment. The concentrations of U and Th within each sample were determined with inductively coupled plasma-mass spectrometry (ICP-MS) and the concentration of K was measured with ICP-optical emission spectrometry (ICP-OES). These analyses were performed by SGS Mineral Services. The alpha and beta dose-rates were calculated using the conversion factors of Liritzis et al. (2013) and the alpha and beta attenuation factors of Brennan et al. (1991) and Guérin et al. (2012), respectively. An internal potassium content of  $12.5 \pm 0.5$  wt% K was assumed for the internal dose-rate (Huntley & Baril, 1997). The environmental dose-rate was calculated using the DRAC software package, v1.2 (Durcan et al., 2015).

### 3.3.2. Sample Preparation, Instrumentation, and Measurement Protocol

Potassium feldspar grains were separated from the collected sediment under dim amber LED lighting conditions at University of California Los Angeles Luminescence Laboratory. Samples were wet sieved to isolate the 175–200  $\mu\text{m}$  size fraction, which was then treated with 3% HCl. Grains with a density  $<2.565$   $\text{g cm}^{-3}$  were separated with lithium metatungstate heavy liquid. Samples were mounted on aluminum single-grain discs and measured using a TL-DA-20 Risø automated reader equipped with a single-grain IR laser (830 nm, at 90% of 150 mW; Bøtter-Jensen et al., 2003) and a  $^{90}\text{Sr}/^{90}\text{Y}$  beta source. Emissions were detected through a Schott BG3-BG39 filter combination.

A p-IR<sub>50</sub> IRSL<sub>225</sub> single-aliquot regenerative (SAR) protocol (Buylaert et al., 2009) was used to determine the equivalent dose  $D_e$  values of individual K-feldspar grains. Following the protocol of Brown et al. (2015), discs were given a regenerative dose and then preheated to 250°C for 60 s. After this preheat, grains were stimulated with an IR laser at 50°C for 3 s each. Because low-temperature IRSL signals are known to suffer from anomalous fading (Huntley & Lamothe, 2001), grains were heated to 225°C for a second IR stimulation, the p-IR IRSL signal, which is generally unaffected by fading (Thomsen et al., 2008). An elevated temperature stimulation with IR diodes at 290°C for 40 s was carried out at the end of each SAR cycle to remove any remaining signal.

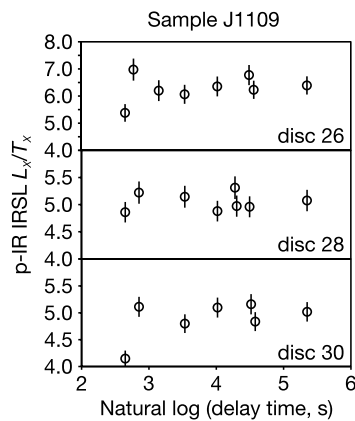


**Figure 3.** Room temperature fading results for three aliquots of sample J1109. On timescales of minutes to several days the p-IR IRSL signal does not fade.

We tested for the presence of athermal fading by administering a beta dose of 10.3 Gy to three small aliquots of J1109, preheating the sample and then allowing the discs to rest at room temperature for delay times ranging from 8 min to 2.5 days. When the delayed luminescence responses were measured, none of the three discs exhibited systematic changes in brightness as a function of storage time (Figure 3), confirming that the p-IR IR225 signal is not fading.

## 4. Results

### 4.1. Ash Wash Fan Age

In the following sections we will refer to several types of ages, implying the timing of a specific geomorphic event. For surface ages derived from cosmogenic nuclide measurements (e.g.,  $^{10}\text{Be}$  and  $^{14}\text{C}$ ), these will always refer to an exposure age. For p-IR IRSL derived ages, these will always refer to the depositional age. For U-series ages, these will refer to the soil pedogenesis age. This usage will be consistent unless otherwise noted.

#### 4.1.1. Surface Exposure Ages

Cosmogenic  $^{14}\text{C}$  and  $^{10}\text{Be}$  concentrations, as well as equivalent exposure ages are summarized in Tables S2 and S3. Amalgamated  $^{10}\text{Be}$  boulder ages previously reported in Blisniuk et al. (2012) are recalculated here using the same scaling and production rate dataset as our new results (Table S2).  $^{14}\text{C}$  exposure dates from the five individual boulders range in age between 4.8 and 10.4 ka. The resulting mean and median  $^{14}\text{C}$  ages are  $7.4 \pm 2.2$  and  $6.6 \pm 1.1$  ka ( $\pm$ half-width interquartile range), respectively. The  $^{10}\text{Be}$  dates from the same samples are consistently older than for  $^{14}\text{C}$  and range between 6.6 and 18.8 ka, with mean and median ages of  $11.8 \pm 4.5$  and  $11.0 \pm 1.6$  ka, respectively. Resulting exposure ages of amalgamated channel bar boulder sets ( $n = 5$ ) yield dates ranging from 9.0 to 12.2 ka, with respective mean and median ages of  $10.7 \pm 1.3$  and  $10.7 \pm 0.8$  ka. Finally, two amalgamated samples from debris flow lobes collected by Blisniuk et al. (2012) to estimate inheritance from the modern channel at Ash Wash yield equivalent  $^{10}\text{Be}$  exposure dates of  $6.5 \pm 0.9$  and  $8.1 \pm 4.4$  ka.

Our results indicate clear systematic differences between nuclides for samples from individual boulders as all  $^{14}\text{C}$  ages are younger than corresponding  $^{10}\text{Be}$  ages. Additionally, the resulting  $^{14}\text{C}$  ages are less scattered than the  $^{10}\text{Be}$  ages. In comparison, the amalgamated samples of Blisniuk et al. (2012) yield a mean  $^{10}\text{Be}$  exposure age similar to the mean of individual boulder  $^{10}\text{Be}$  ages reported here; however, the results from the five amalgamated samples are less scattered than the five individual boulder samples for either nuclide (Figure 4). This is likely because the amalgamated samples from a total of 25 boulder surfaces ( $\sim 5$  boulder tops per amalgamated sample) approximate more closely the real population statistics compared to only five total samples for the individual boulder, regardless of the nuclide measured. Sampling an equivalent number of individual boulder surfaces is likely to resemble similar population statistics as expressed in the amalgamated samples. Also, apparent is that amalgamating surface samples does not necessarily minimize  $^{10}\text{Be}$  inheritance. This is not to say that either individual boulder samples or amalgamated samples is a superior method, and neither are necessarily representative of the true depositional age. It instead indicates that amalgamating samples is an efficient way to represent the population mean of exposure ages from an alluvial fan more robustly than a few individual measurements, while the distribution of individual boulder samples may yield insight into sediment transport processes (see Section 5 below).

#### 4.1.2. IRSL Depositional Ages

Radial plots (Galbraith et al., 1999) of single grain equivalent dose ( $D_e$ ) values are shown for all four samples in Figure 5. Sample J1109 exhibits an overdispersion value of 30%, which is relatively low for single grain p-IR<sub>50</sub> IR<sub>225</sub> dating (e.g., Malatesta et al., 2017). The overdispersion parameter represents the spread in single grain  $D_e$  values in excess of the individual measurement uncertainty values (Galbraith et al., 1999). A single, well-bleached population of grains should therefore cluster around a common burial dose with low variance, and variance beyond some geomorphically reasonable threshold value (e.g.,  $20 \pm 9\%$  for single-grain



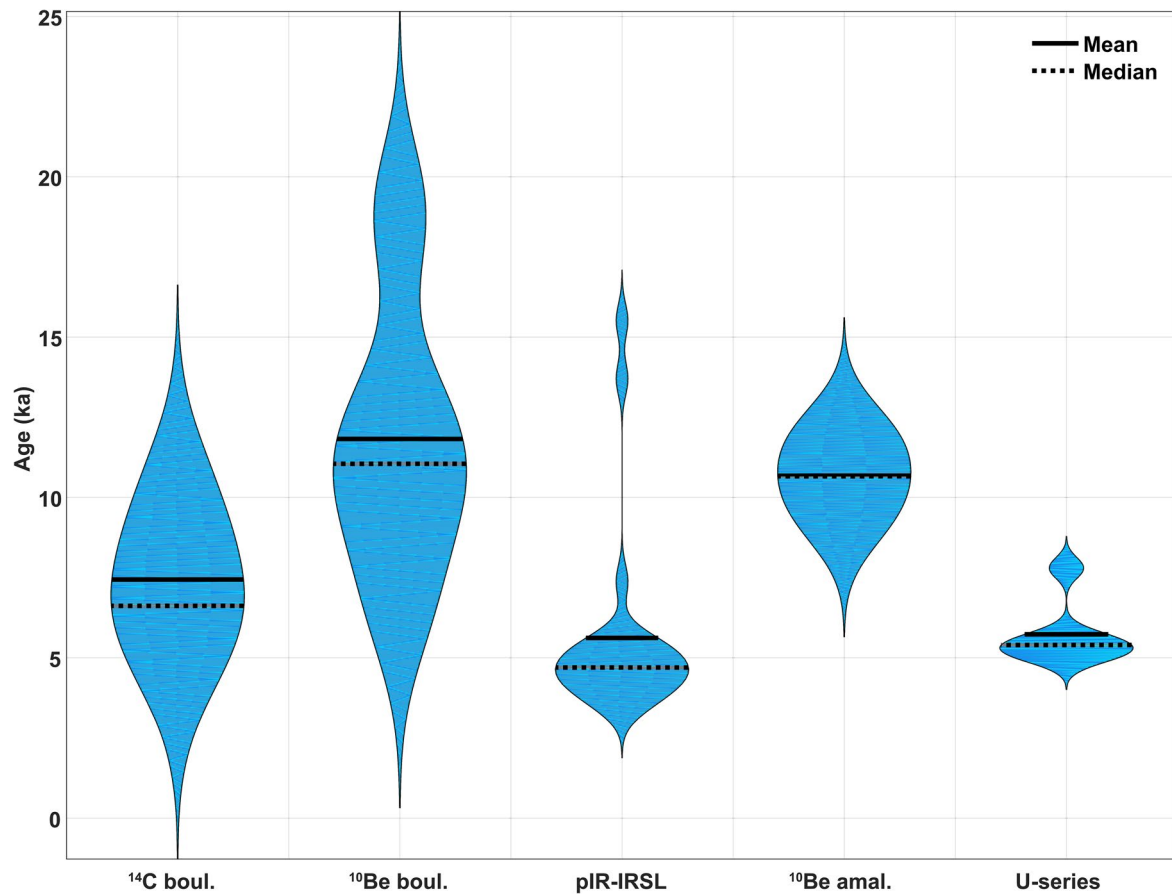


**Figure 4.** Violin plots showing the mean (black heavy line), median (black dashed line), and kernel density estimates for the age of fan Q3b using various geochronometers. For the cosmogenic and U-series methods, individual sample ages were used. For pIR-IRSL, the distribution of equivalent doses from J1109 was used as a proxy for kernel density estimates of ages.

quartz deposits; Arnold & Roberts, 2009) can indicate that a sample represents a single poorly bleached population or multiple dose populations. In contrast to J1109, samples J1110, J1111, and J1112 exhibit more  $D_e$  overdispersion than is expected for a single population, with values of 54%, 60%, and 79%. Sample J1109 is interpreted using the central age model, which estimates the age of a single dose population (Galbraith et al., 1999). The other samples are assumed to incorporate some grains with sufficient sunlight exposure and others that were insufficiently bleached before burial. These samples are interpreted using the three-parameter minimum age model (Galbraith et al., 1999), assuming an overdispersion of 15%, typical for similar sediments in the region (Rhodes, 2015) and consistent with the OD of  $13.6 \pm 1.8\%$  measured in the dose recovery test (see Supporting Information S1). The resulting burial doses and ages for each of the samples are shown in Table S4.

Of these four samples, only J1109 was collected from within the Q3b fan surface targeted by the other geochronometers in this study. The central age model for this sample is  $5.3 \pm 0.5$  ka ( $\pm 1\sigma$ ). Our high confidence in this age is due to the relatively low single grain  $D_e$  overdispersion (30%) and the absence of fading during laboratory measurements. Because the overdispersion for this sample is low, we expect partial bleaching effects to be insignificant.

The remaining samples (J1110, J1111, and J1112) are all from small inset terraces within the Q3b surface which discontinuously infill the modern channel network, elevated above the active channel by tens of cm to about 1 m. These deposits range in age from 0.8 to 1.4 ka and exhibit highly dispersed  $D_e$  values indicating incomplete bleaching prior to deposition.

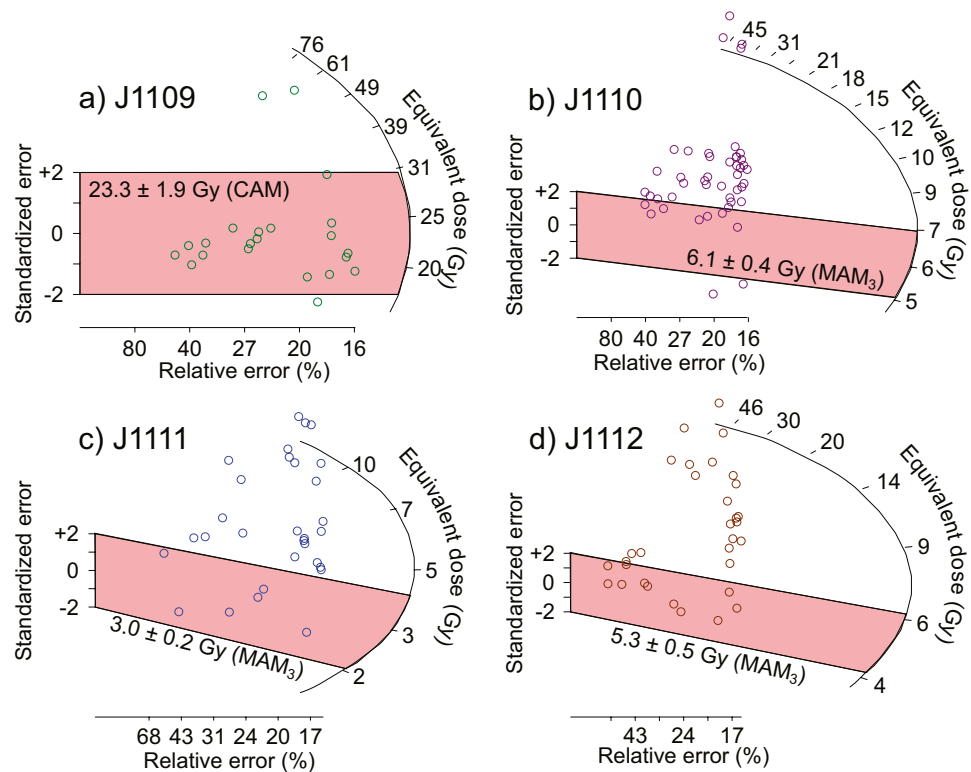


**Figure 5.** Radial plots showing the single-grain equivalent dose distributions for each sample. The chosen age models are highlighted in pink.

### 4.1.3. Summary of Ash Wash Fan Age

In our dataset, regardless of the cosmogenic nuclide, inheritance from prior exposure is more the norm rather than the exception. The fact that there is apparent  $^{14}\text{C}$  inheritance ( $7.4 \pm 2.2$  ka), albeit within uncertainties of the other methods, compared to the Q3b surface age from p-IR IRSL ( $5.3 \pm 0.5$  ka) and U-series dating of pedogenic carbonates ( $5.2 \pm 0.3$  ka) suggests that storage at depths deep enough to minimize production is short and thus transport is relatively rapid from catchment to the fan surface. This is consistent with the expected behavior for sediment delivered to an arid alluvial fan. The resulting  $^{10}\text{Be}$  exposure ages regardless of sampling approach all display greater amounts of inheritance than  $^{14}\text{C}$  does. At this point, when the sampling of material allows, p-IR IRSL and U-series provide the most robust chronology for alluvial fan surfaces, such as those at Ash Wash.

## 5. Discussion

### 5.1. A Multi-Chronometer History of Alluvial Fan Sediment

In our discussion below we assume that relative to the age of the fan surface, sediment accumulation during fan formation is rapid, and thus ages resulting from our multi-chronometer approach should be concordant.

The  $^{14}\text{C}$  exposure ages are systematically younger than  $^{10}\text{Be}$  exposure ages from the same samples, which is also borne out by the  $^{14}\text{C}$  and  $^{10}\text{Be}$  concentrations. Figure 6 shows the  $^{14}\text{C}$  and  $^{10}\text{Be}$  concentrations on a paired nuclide plot. All samples are consistent with continuous exposure and steady-state erosion at  $2\sigma$  uncertainty. Regardless, the general trend is that all samples are closer to the field of complex exposure than to simple continuous single-stage exposure. This can be interpreted in two end-member ways. The first is that samples are shifted toward the field of complex exposure (i.e., burial) due to  $^{10}\text{Be}$  inheritance solely, which will serve to lower the resulting  $^{14}\text{C}$ - $^{10}\text{Be}$  ratio below that expected for continuous exposure (eroding or not eroding). The second is that the samples experienced a period of burial during the Holocene, but after deposition on the Q3b surface. We disregard a third possibility here, that of continuous exposure with

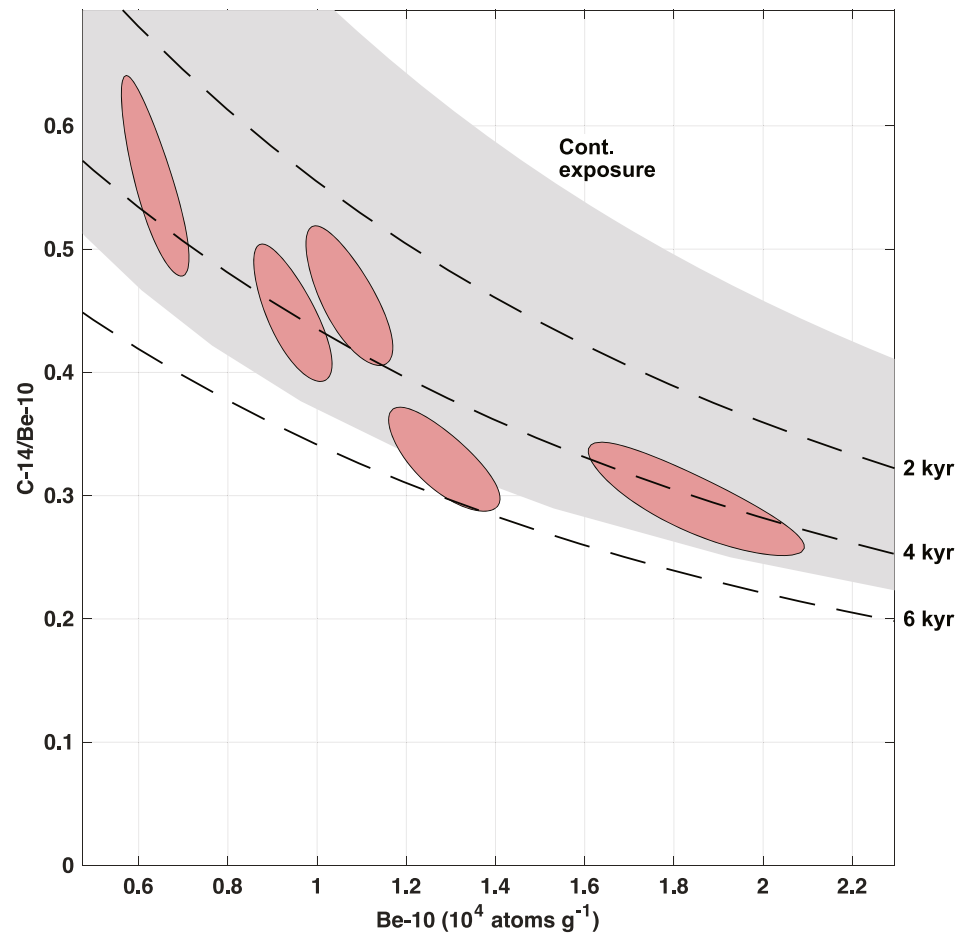


**Figure 6.** Paired  $^{14}\text{C}$ – $^{10}\text{Be}$  nuclide plot for the individual boulder samples from the Ash Wash fan surface. Gray shading represents the continuous exposure steady state erosion island, with the upper-bound being the continuous exposure no erosion trajectory, meaning measured concentrations are consistent with continuous exposure while steadily eroding. Samples plotting below the steady state erosion can be interpreted as having experienced one or more period of burial and shielding from the cosmic ray flux. One standard deviation error ellipse for each sample is shown in red. Dashed lines are burial isochrons for 2, 4, and 6 Kyr. Nuclide concentrations are normalized to unit production ( $1 \text{ atoms g}^{-1} \text{ yr}^{-1}$ ) to facilitate the comparison of samples from different elevations.

steady state erosion primarily because the decay systematics of  $^{14}\text{C}$  require boulder surface erosion rates ( $75\text{--}240 \text{ m Myr}^{-1}$ ) higher than is realistic for Anza Borrego during the Holocene (ca.  $30 \text{ m Myr}^{-1}$ ; Owen et al., 2011). Given that all samples in this study are from highs on alluvial fan channel bars, all surfaces are relatively fresh, and there is no evidence for sediment burial after deposition of the fan surface, we can largely rule out the second scenario. The most likely scenario is that boulders record a multi-stage exposure history that reflects accumulation of nuclides from higher elevations in the Ash Wash catchment, one or more periods of sediment storage during which nuclides decay ( $^{14}\text{C}$  decay  $\gg$   $^{10}\text{Be}$  decay) more than accumulate, and finally deposition on the Ash Wash fan surface. Implied in this is rapid transport at the surface in high-energy debris flows. The presence of  $^{14}\text{C}$  inheritance, as inferred from the younger U-series (Blisniuk et al., 2012) and p-IR IRSL ages, while simultaneously having  $^{14}\text{C}/^{10}\text{Be}$  ratios below the field of continuous exposure indicates that there were storage periods where boulders were buried with reduced production rates.

### 5.1.1. Inferred Sediment Transport and Storage History From Paired Cosmogenic Nuclides

Here, we take advantage of inherited  $^{14}\text{C}$  and  $^{10}\text{Be}$  concentrations and depositional ages inferred from U-series and p-IR IRSL ages to derive estimates of the prior exposure and storage time of the boulders prior to deposition on the fan. Implicit in this approach is that we are assuming the U-series and p-IR IRSL ages

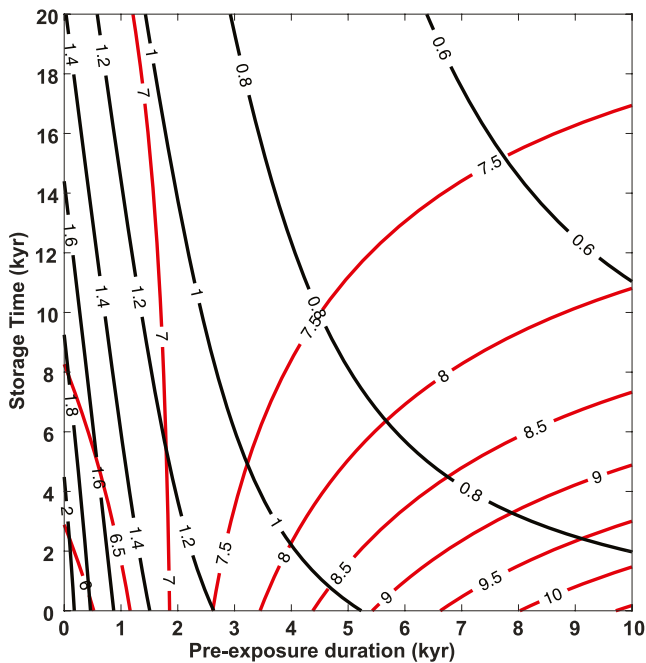


**Figure 7.** Modeled resulting  $^{14}\text{C}$  concentrations (red contours of  $10^4$  atoms  $\text{g}^{-1}$ ) and  $^{14}\text{C}$ - $^{10}\text{Be}$  ratios (black) for samples from the Ash Wash fan assuming  $\sim 5.3$  ka actual fan age derived from IRSL and U-series. The axes explore a range of prior exposure durations in the catchment and storage during transport to the fan, assuming storage depths of 1 m. The model suggests that only a narrow range of prior exposure durations and relatively short burial are allowed. The max prior exposure duration is set by the oldest apparent  $^{10}\text{Be}$  age.

are correlative or close to the true age of the Q3b surface aggradation. In this case, we are referring to prior exposure as the time spent *in situ* as bedrock and assume zero erosion, while burial is loosely defined as the time spent during transport as sediment not at the surface, but not necessarily deep burial ( $>2$  m) where production is effectively zero. The measured  $^{14}\text{C}$  and  $^{10}\text{Be}$  concentrations, as well as the  $^{14}\text{C}$ - $^{10}\text{Be}$  ratio are the result of a three-stage history of integrated prior exposure duration, storage duration, and most recent exposure duration. The latter we know from the U-series and p-IR IRSL measurements, assuming that the boulder emplacement age is indistinguishable from the fan aggradation age. We can thus write an equation for each sample describing the measured concentrations,  $N$ , for each nuclide,  $j$ , as follows

$$N_j = \frac{1}{\lambda_j} \left[ P_{j,\text{prior}} \left( 1 - e^{-t_{\text{prior}}\lambda_j} \right) e^{-(t_{\text{stor}}+t_{\text{post}})\lambda_j} + P_{j,\text{stor}} e^{-z\rho/\lambda_j} \left( 1 - e^{-t_{\text{stor}}\lambda_j} \right) e^{-t_{\text{post}}\lambda_j} + P_{j,\text{post}} \left( 1 - e^{-t_{\text{post}}\lambda_j} \right) \right], \quad (1)$$

where  $P$ ,  $\lambda$ ,  $z$ ,  $\rho$ , and  $\Lambda$  are the respective production rates (atoms  $\text{g}^{-1} \text{yr}^{-1}$ ), decay constant ( $\text{yr}^{-1}$ ), depth of storage (cm), overburden density ( $\text{g cm}^{-3}$ ), and attenuation length ( $\text{g cm}^{-2}$ ) for each nuclide. Additionally,  $t_{\text{prior}}$  is the prior exposure duration,  $t_{\text{stor}}$  the duration of storage, and  $t_{\text{post}}$  the most recent exposure period. The resulting nuclide ratio can be described by the ratio of the equation describing  $^{14}\text{C}$  to that for  $^{10}\text{Be}$ . In this model, we assume that transport is instantaneous relative to the time scales of prior exposure, storage, and exposure on the alluvial fan, and therefore there is no significant accumulation via production or loss of nuclides via decay during transport. Thus, we assume that during the prior exposure period, erosion is negligible, similar to assumptions made in calculating simple exposure ages. This assumption is justified by the observation that  $^{14}\text{C}$  is insensitive to all but the highest of erosion rates and dominantly sets the observed concentration and nuclide ratio signals (Figure 7). Finally, the

production rates for prior exposure, storage, and deposition are all different as a result of the sample transiting a range of elevations and shielding depths during storage.

Considering the above, we can generate modeled  $^{14}\text{C}$  concentrations and  $^{14}\text{C}$ - $^{10}\text{Be}$  ratios for a range of storage and prior exposure durations by making basic assumptions regarding the elevations of prior exposure and storage for our Q3b surface (Figure 7; Table S5). Our results lead to first-order observations regarding the resulting  $^{14}\text{C}$  concentrations. First  $^{14}\text{C}$  concentrations are nearly invariant with respect to storage time when prior exposure durations are less than  $\sim 2$  Kyr. Second, as prior exposure duration increases the  $^{14}\text{C}$  concentration becomes highly dependent on the duration of storage prior to final deposition. Third, the measured  $^{14}\text{C}$ - $^{10}\text{Be}$  ratio strongly depends on the storage duration for all but the shortest prior exposure durations because  $^{10}\text{Be}$  is effectively stable over the Holocene and thus the ratio is essentially entirely dependent on  $^{14}\text{C}$  decay. For the scenarios above, increasing the depth of storage will enhance the observed invariance, decrease the overall dependence on prior exposure duration, and increase  $^{14}\text{C}$ - $^{10}\text{Be}$  ratio sensitivity as the sample becomes more completely shielded and decay dominates. Finally, because of the relatively short time to production-decay steady state equilibria (i.e., saturation) for  $^{14}\text{C}$ , fan surfaces older than ca. 26 ka will have  $^{14}\text{C}$  concentrations that begin to approach saturation regardless of the upstream history as all previously accumulated nuclides will have decayed away.

Our simple model suggests that solutions to solve for prior exposure and storage duration exist, and is furthermore borne out mathematically, where we have two unknowns ( $t_{\text{pre}}$  and  $t_{\text{stor}}$ ) and two equations. However, uncertainties associated with nuclide measurements and production parameters means that there is a suite of solutions for  $t_{\text{pre}}$  and  $t_{\text{stor}}$ . We therefore take a bootstrap Monte Carlo approach to derive prior exposure and storage durations for each Q3b surface sample. For each sample, we assume Gaussian uncertainties on the  $^{14}\text{C}$  concentrations and  $^{14}\text{C}$ - $^{10}\text{Be}$  ratio. We use the composite average of the U-series and p-IR IRSL ages as  $t_{\text{post}}$  and

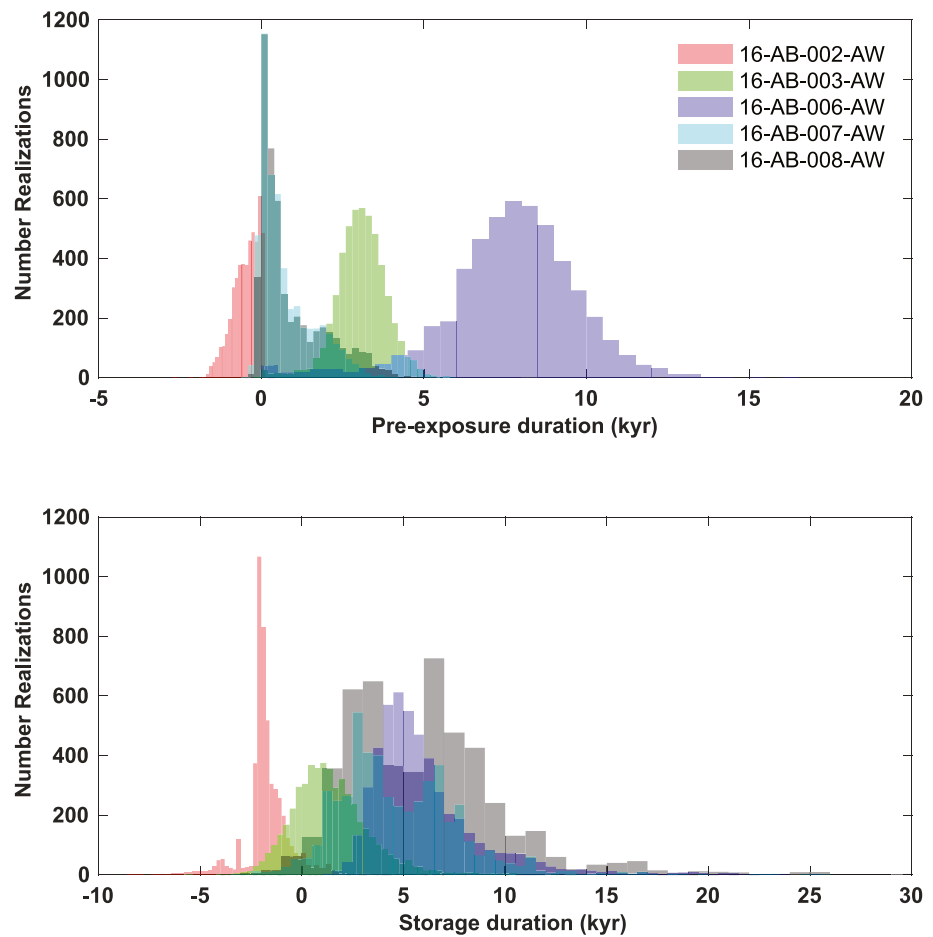


**Figure 8.** Estimates of prior exposure duration for the sampled boulders (top) and estimates of the storage duration for the sampled boulders based on the measured in situ  $^{14}\text{C}$  and  $^{10}\text{Be}$ . Prior exposure durations vary widely between 0 and 10 Kyr, while storage durations cluster around 5 Kyr except for one sample.

additionally assume Gaussian uncertainty for the age distribution based on the standard deviation from the U-series and p-IR IRSL ages when combined. Finally, we need to make assumptions regarding the depth of burial during storage. There is little evidence for deep burial ( $>2$  m) in channel bank deposits that would result in complete shielding of the sample during transport from the catchment to the fan surface. Therefore, we assume that the depth of burial is log-normally distributed with a mean of 100 cm and standard deviation of 50 cm; this approach thus favors shallow burial but does not preclude occasional deep burial. For each sample, we determine values of  $t_{\text{pre}}$  and  $t_{\text{stor}}$  for 5,000 realizations by minimizing the difference between the modeled and measured  $^{14}\text{C}$  concentrations and  $^{14}\text{C}$ - $^{10}\text{Be}$  ratios using the MATLAB fsolve non-linear equation solver routine. The advantage of the Monte Carlo approach here is that we can assess the impact on the model results ( $t_{\text{post}}$  and  $t_{\text{pre}}$ ) from measurement uncertainty and geomorphic model parameter distributions.

Results from modeling prior exposure and storage durations are shown in Figure 8. All samples except for 16-AB-002-AW require prior exposure durations greater than zero. The resulting distributions are largely Gaussian except for those near zero, where the distributions are strongly skewed to the right. Mean prior exposure durations range between 0.73 and 7.7 Kyr with an overall mean of  $3.1 \pm 3.2$  Kyr. In contrast, the modeled storage durations are generally all Gaussian-like in form and are less-spread than the prior exposure duration ranging from 1.4 to 6.2 Kyr with an overall mean of  $4.6 \pm 2.2$  Kyr. Similar to the prior exposure duration, a negative storage duration is required to fit the resulting concentrations and ratios for 16-AB-002-AW. This result is because the measured  $^{14}\text{C}$  concentration and  $^{14}\text{C}$ - $^{10}\text{Be}$  ratio is less than and greater than, respectively, that required for the 5.3 ka age of the fan used in our model derived from p-IR IRSL and U-series methods. The apparent  $^{14}\text{C}$  exposure age for 002-AW is  $4.8 \pm 0.2$  Kyr, slightly less than the p-IR

IRSL and U-series ages, but in overall agreement within  $2\sigma$  uncertainties. The slightly younger exposure age may result from that particular cobble being deposited during the latest stage of Q3b activity and therefore would post-date the sediment burial age of the p-IR IRSL sample collected 1.4 m below the Q3b surface and initial pedogenic carbonate rind formation. However, in general, the three chronometers are in agreement and the slightly younger  $^{14}\text{C}$  exposure age may simply be a result of the typical spread associated with any distribution of exposure ages of an alluvial fan surface (e.g., Heyman et al., 2011).

### 5.1.2. Inferred Sedimentary Storage Duration Based on Single-Grain IRSL Age Populations

Single-grain p-IR IRSL apparent age distributions are usually reduced to a single modeled age, the age since the last sunlight exposure, even though significant age variance between grains may exist within a single sample. If grain ages are highly scattered, the assumptions usually made is that some grains were unbleached or partially bleached prior to burial while some were exposed to sunlight long enough to fully bleach before their most recent burial, or that deposit heterogeneity results in beta-dose heterogeneity. Under this assumption, the minimum age model is typically applied to summarize the age of the youngest grains in the distribution (Galbraith et al., 1999).

In addition to the most recent burial duration, the single grain ages within a sediment sample may contain additional information about sediment storage intervals. If some grains were unbleached during the most recent depositional event, those grains could yield an age corresponding to a previous sunlight exposure event. In this way, a fluvial environment which fully bleaches only some grains during transport (Gray et al., 2018; McGuire & Rhodes, 2015) events may produce single-grain age populations which record multiple sunlight exposure events, assuming similar dose rate environments during burial (Gray et al., 2017; Saha et al., 2021). This approach assumes complete bleaching of some grains during each event. If this assumption is violated, none of the grains would record the bleaching event. We suspect this effect is minor because age clusters shared between samples are apparent, which we would not expect were each sample partially bleached to an arbitrary degree. To investigate this possibility, we apply the finite mixture model (Galbraith & Green, 1990) within the R Luminescence package (Kreutzer et al., 2012) to all luminescence samples. This model estimates the ages of discrete age populations within each distribution. The optimum number of age components is chosen by minimizing the Bayesian Information Criterion.

These age components are shown in Figure 9a, shown as a function of the youngest component age per sample, which is assumed to be the most recent depositional event. In Figure 9b, the time interval between adjacent age components is shown, also as a function of the youngest component age. The sample taken from the Q3b deposit, J1109, is outlined with a dashed blue box, while all other samples are from the younger inset terraces adjacent.

The time interval between age populations should approximate the storage time of sediment before remobilization. To summarize these intervals for all samples together, we adopt a bootstrap Monte Carlo approach. For each sample, we randomly sample from the youngest age component, a Gaussian distribution defined by the age and  $1\sigma$  error. Next, we sample from the second-youngest population to define duration of the burial interval. This is done  $10^5$  times for every adjacent population. The resulting histograms of these burial intervals are illustrated, combined (Figure 9c) and separately (Figure 9d). These results suggest that sediments within this catchment are often buried for  $\sim 2$  or 10 ka before remobilization.

### 5.1.3. Summary of Inferred Sediment Transport and Deposition History

The results of sediment storage durations prior to ultimate deposition on/in the alluvial fan are highly consistent for both the cosmogenic nuclide and p-IR IRSL methods with durations between 0 and 10 Kyr. Results based on cosmogenic nuclides suggest that either the sediment is stored in the landscape for  $\sim 5$  Kyr or has little to no storage; the resulting prior exposure time before transport varies widely. Conversely, the IRSL results suggest that storage duration is bimodal with peaks at  $\sim 2$  and 10 Kyr. The different storage durations from the two methods suggests that the timescale of storage is possibly grain size dependent, and therefore process dependent. As sampled the two methods require fundamentally different grain sizes, sand for p-IR IRSL and cobbles and boulders for cosmogenic nuclides, and therefore our limited dataset precludes any stronger conclusions regarding grain size dependency on storage time or sediment source. The IRSL storage mode at 2 Kyr is only observed for late Holocene samples from inset terraces and could indicate that storms capable of mobilizing large packages of sand occur more frequently or more recently than storms with

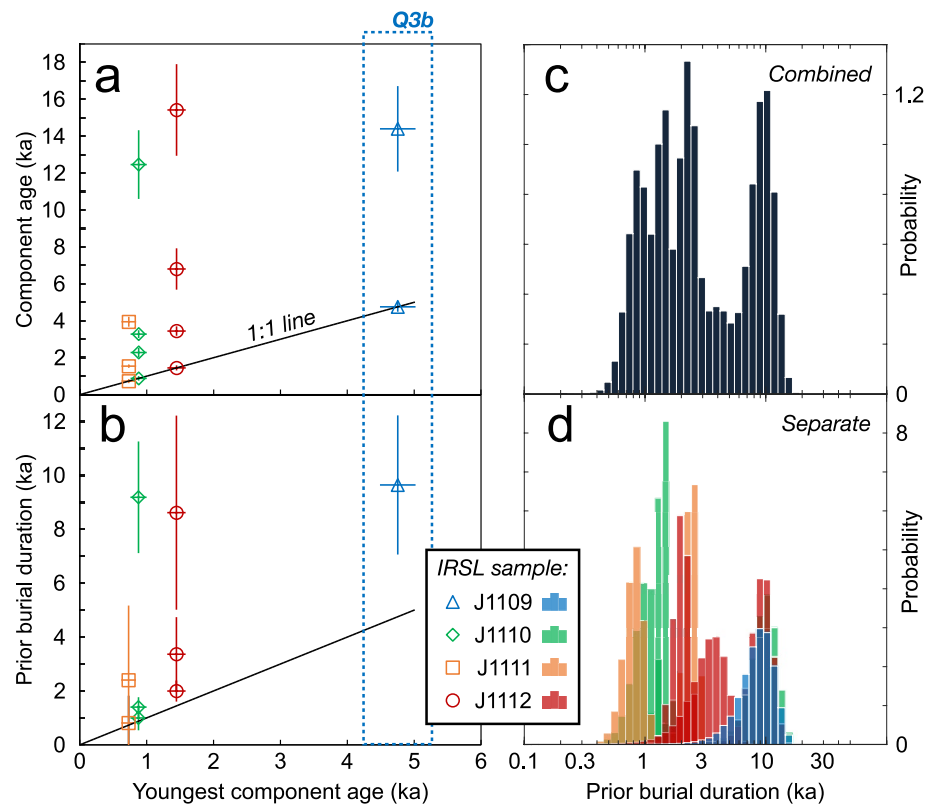


**Figure 9.** IRSL component ages (a) and prior burial durations (b) shown per sample, sorted by the youngest component age of each sample. Burial duration estimates for (c) all samples combined and (d) each sample treated separately. Results suggest in both scenarios that samples are buried before final deposition for either ~2 or 10 Kyr.

sufficient transport capacity to mobilize boulders. The mode at 10 ka (Figure 9a) that was followed by quiescence for about 10 Kyr. Measurement of *in situ*  $^{14}\text{C}$  and  $^{10}\text{Be}$  from sand to test grain size dependence (e.g., Fülöp et al., 2020; Hippe et al., 2018; Lukens et al., 2016) or p-IR IRSL dating of the undersides of boulders (e.g., Brill et al., 2020; Freiesleben et al., 2015) would be informative. Regardless, our results suggest that sand grains within a catchment experience multiple storage histories, while cobbles and boulders given their quasi-normally distributed storage durations all behave similarly within the landscape prior to final deposition on the fan surface. This interpretation is not without merit, as analysis of the median grain size for fans of Pleistocene and Holocene age indicate differences likely tied to precipitation (Brooke et al., 2018). Similarly, work applying the methods presented here will best be combined with detailed sedimentologic description and grain size distributions characterized.

## 6. Conclusions

We have shown the benefit of a multi-chronometer approach, each of which commence their clock in response to different geomorphic events, to explore the dating of alluvial fan surfaces and to understand the prior depositional history of sediment delivered to an alluvial fan. *In situ*  $^{14}\text{C}$  is more effective than  $^{10}\text{Be}$  for surface exposure dating of young features but is not completely free of inheritance. IRSL of the sand fraction from the same fan surface shows high repeatability between grains and is in excellent agreement with U-series ages of pedogenic carbonates.

We have also shown that *in situ*  $^{14}\text{C}$  and  $^{10}\text{Be}$  inheritance preserves a record of the integrated prior exposure and storage duration for a given boulder sample that can be extracted if the depositional age is known independently (i.e., from IRSL or U-series). Application of a finite mixture model to IRSL grain populations also shows that sand is deposited with a record of storage manifest as incomplete resetting. Our two independent methods thus provide insight into the storage duration that a given grain size (cobbles/boulders vs. sand)

experiences prior to final deposition. Both cobbles/boulders and sand tend to have bi-modal distributions of storage time, but the main modes are different for the different grain sizes.

## Data Availability Statement

All data reported and MATLAB code used in this manuscript is archived in a UT-Arlington Data Repository and can be accessed at <https://doi.org/10.18738/T8/1XGF5H>.

## Acknowledgments

This work was funded in part by grants from the Southern California Earthquake Center to BMG and NSF-EAR 1728145 to SM. The staffs of Lawrence Livermore National Lab Center for Accelerator Mass Spectrometry and Purdue University Rare Isotope Measurement Laboratory are thanked for their excellent measurements. BMG thanks Keir Nichols and Rachel Sortor with field work assistance; Chandler Powers for sample preparation and quartz isolation. We acknowledge the land we worked on is the ancestral and current home of the Chuilla and Xawill kw̓ichawaay (Cocopah). Finally, we thank comments and suggestions from four reviewers and associate editor Harrison Gray that improved this article.

## References

- Allen, P. A., & Densmore, A. L. (2000). Sediment flux from an uplifting fault block. *Basin Research*, 12(3–4), 367–380. <https://doi.org/10.1111/j.1365-2117.2000.00135.x>
- Anderson, R. S., Repka, J. L., & Dick, G. S. (1996). Explicit treatment of inheritance in dating depositional surfaces using in situ <sup>10</sup>Be and <sup>26</sup>Al. *Geology*, 24(1), 47–51. [https://doi.org/10.1130/0091-7613\(1996\)024<0047:etoidd>2.3.co;2](https://doi.org/10.1130/0091-7613(1996)024<0047:etoidd>2.3.co;2)
- Antinao, J. L., McDonald, E., Rhodes, E. J., Brown, N., Barrera, W., Gosse, J. C., & Zimmerman, S. (2016). Late Pleistocene-Holocene alluvial stratigraphy of southern Baja California, Mexico. *Quaternary Science Reviews*, 146, 161–181. <https://doi.org/10.1016/j.quascirev.2016.06.008>
- Arnold, L. J., & Roberts, R. G. (2009). Stochastic modelling of multi-grain equivalent dose (De) distributions: Implications for OSL dating of sediment mixtures. *Quaternary Geochronology*, 4, 204–230. <https://doi.org/10.1016/j.quageo.2008.12.001>
- Axen, G. J., & Fletcher, J. M. (1998). Late Miocene-Pleistocene extensional faulting, northern Gulf of California, Mexico and Salton Trough, California. *International Geology Review*, 40(3), 217–244. <https://doi.org/10.1080/00206819809465207>
- Balco, G. (2017). Production rate calculations for cosmic-ray-muon-produced <sup>10</sup>Be and <sup>26</sup>Al benchmarked against geological calibration data. *Quaternary Geochronology*, 39, 150–173. <https://doi.org/10.1016/j.quageo.2017.02.001>
- Blisniuk, K., Oskin, M., Fletcher, K., Rockwell, T., & Sharp, W. (2012). Assessing the reliability of U-series and <sup>10</sup>Be dating techniques on alluvial fans in the Anza Borrego Desert, California. *Quaternary Geochronology*, 13(c), 26–41. <https://doi.org/10.1016/j.quageo.2012.08.004>
- Borchers, B., Marrero, S., Balco, G., Caffee, M., Goehring, B., Lifton, N., et al. (2016). Geological calibration of spallation production rates in the CRONUS-Earth project. *Quaternary Geochronology*, 31, 188–198. <https://doi.org/10.1016/j.quageo.2015.01.009>
- Bøtter-Jensen, L., Andersen, C. E., Duller, G. A. T., & Murray, A. S. (2003). Developments in radiation, stimulation and observation facilities in luminescence measurements. *Radiation Measurements*, 37, 535–541.
- Brennan, B. J., Lyons, R. G., & Phillips, S. W. (1991). Attenuation of alpha particle track dose for spherical grains. *Nuclear Tracks and Radiation Measurements*, 18, 249–253. [https://doi.org/10.1016/1359-0189\(91\)90119-3](https://doi.org/10.1016/1359-0189(91)90119-3)
- Brill, D., May, S. M., Mhammedi, N., King, G., Burrow, C., Wolf, D., et al. (2020). OSL rock surface exposure dating as a novel approach for reconstructing transport histories of coastal boulders over decadal to centennial timescales. *Earth Surface Dynamics*, 2020, 1–44. <https://doi.org/10.5194/esurf-2020-46>
- Brooke, S. A. S., Whittaker, A. C., Armitage, J. J., D'Arcy, M., & Watkins, S. E. (2018). Quantifying sediment transport dynamics on alluvial fans from spatial and temporal changes in grain size, Death Valley, California. *Journal of Geophysical Research: Earth Surface*, 123(8), 2039–2067. <https://doi.org/10.1029/2018j004622>
- Brown, N. D. (2020). Which geomorphic processes can be informed by luminescence measurements? *Geomorphology*, 367, 107296. <https://doi.org/10.1016/j.geomorph.2020.107296>
- Brown, N. D., Rhodes, E. J., Antinao, J. L., & McDonald, E. V. (2015). Single-grain post-IR IRSL signals of K-feldspars from alluvial fan deposits in Baja California Sur, Mexico. *Quaternary International*, 362, 132–138. <https://doi.org/10.1016/j.quaint.2014.10.024>
- Buylaert, J. P., Murray, A. S., Thomsen, K. J., & Jain, M. (2009). Testing the potential of an elevated temperature IRSL signal from K-feldspar. *Radiation Measurements*, 44(5–6), 560–565. <https://doi.org/10.1016/j.radmeas.2009.02.007>
- Colarossi, D., Duller, G. A. T., Roberts, H. M., Tooth, S., & Lyons, R. (2015). Comparison of paired quartz OSL and feldspar post-IR IRSL dose distributions in poorly bleached fluvial sediments from South Africa. *Quaternary Geochronology*, 30, 233–238. <https://doi.org/10.1016/j.quageo.2015.02.015>
- D'Arcy, M. K., Schildgen, T. F., Turowski, J. M., & DiNezio, P. (2019). Inferring the timing of abandonment of aggraded alluvial surfaces dated with cosmogenic nuclides. *Earth Surface Dynamics*, 7(3), 755–771. <https://doi.org/10.5194/esurf-7-755-2019>
- Dibblee, T. W., & Mich, J. A. (2008). *Geologic map of the Clark Lake & Rabbit Peak 15 minute quadrangles, Riverside, San Diego, and Imperial Counties*. California: Diblee Geological Foundation.
- Ditchburn, R. G., & Whitehead, N. E. (1994). The separation of <sup>10</sup>Be from silicates. Proceedings of the 3rd Workshop of the South Pacific Environmental Radioactivity Association (SPERA) Extended Abstracts. Canberra, Australia.
- Dorn, R. I. (1994). The role of climatic change in alluvial fan development. In A. D. Abrahams & A. J. Parsons (Eds.), *Geomorphology of desert environments* (pp. 593–615). Dordrecht: Springer. [https://doi.org/10.1007/978-94-015-8254-4\\_23](https://doi.org/10.1007/978-94-015-8254-4_23)
- Dühnforth, M., Densmore, A. L., Ivy-Ochs, S., Allen, P., & Kubik, P. W. (2017). Early to Late Pleistocene history of debris-flow fan evolution in western Death Valley (California) using cosmogenic <sup>10</sup>Be and <sup>26</sup>Al. *Geomorphology*, 281, 53–65. <https://doi.org/10.1016/j.geomorph.2016.12.020>
- Durcan, J. A., King, G. E., & Duller, G. A. T. (2015). DRAC: Dose rate and age calculator for trapped charge dating. *Quaternary Geochronology*, 28, 54–61. <https://doi.org/10.1016/j.quageo.2015.03.012>
- Foster, M. A., Anderson, R. S., Gray, H. J., & Mahan, S. A. (2017). Dating of river terraces along Lefthand Creek, western High Plains, Colorado, reveals punctuated incision. *Geomorphology*, 295, 176–190. <https://doi.org/10.1016/j.geomorph.2017.04.044>
- Frankel, K. L., Brantley, K. S., Dolan, J. F., Finkel, R. C., Klinger, R. E., Knott, J. R., et al. (2007). Cosmogenic <sup>10</sup>Be and <sup>36</sup>Cl geochronology of offset alluvial fans along the northern Death Valley fault zone: Implications for transient strain in the eastern California shear zone. *Journal of Geophysical Research*, 112(B6), 18. <https://doi.org/10.1029/2006JB004350>
- Freiesleben, T., Sohbaty, R., Murray, A., Jain, M., al Khasawneh, S., Hvidt, S., & Jakobsen, B. (2015). Mathematical model quantifies multiple daylight exposure and burial events for rock surfaces using luminescence dating. *Radiation Measurements*, 81, 16–22. <https://doi.org/10.1016/j.radmeas.2015.02.004>



- Fülöp, R. H., Codilean, A. T., Wilcken, K. M., Cohen, T. J., Fink, D., Smith, A. M., et al. (2020). Million-year lag times in a post-orogenic sediment conveyor. *Science Advances*, *6*(25), eaaz8845. <https://doi.org/10.1126/sciadv.aaz8845>
- Galbraith, R. F., & Green, P. F. (1990). Estimating the component ages in a finite mixture. *International Journal of Radiation Applications and Instrumentation. Part D: Nuclear Tracks and Radiation Measurements*, *17*(3), 197–206. [https://doi.org/10.1016/1359-0189\(90\)90035-v](https://doi.org/10.1016/1359-0189(90)90035-v)
- Galbraith, R. F., Roberts, R. G., Laslett, G. M., Yoshida, H., & Olley, J. M. (1999). Optical dating of single and multiple grains of quartz from Jinmium rock shelter, northern Australia: Part I, experimental design and statistical models. *Archaeometry*, *41*(2), 339–364. <https://doi.org/10.1111/j.1475-4754.1999.tb00987.x>
- Gliganic, L. A., Cohen, T. J., Meyer, M., & Molenaar, A. (2017). Variations in luminescence properties of quartz and feldspar from modern fluvial sediments in three rivers. *Quaternary Geochronology*, *41*, 70–82. <https://doi.org/10.1016/j.quageo.2017.06.005>
- Goehring, B. M., Schimmelpfennig, I., & Schaefer, J. M. (2014). Capabilities of the Lamont–Doherty Earth Observatory in situ <sup>14</sup>C extraction laboratory updated. *Quaternary Geochronology*, *19*, 194–197. <https://doi.org/10.1016/j.quageo.2013.01.004>
- Goehring, B. M., Wilson, J., & Nichols, K. (2019). A fully automated system for the extraction of in situ cosmogenic carbon-14 in the Tulane University cosmogenic nuclide laboratory. *Nuclear Instruments and Methods in Physics Research, Section B: Beam Interactions With Materials and Atoms*, *455*, 284–292. <https://doi.org/10.1016/j.nimb.2019.02.006>
- Gray, H. J., Jain, M., Sawakuchi, A. O., Mahan, S. A., & Tucker, G. E. (2019). Luminescence as a sediment tracer and provenance tool. *Reviews of Geophysics*, *57*, 987–1017. <https://doi.org/10.1029/2019RG000646>
- Gray, H. J., Tucker, G. E., & Mahan, S. A. (2018). Application of a luminescence-based sediment transport model. *Geophysical Research Letters*, *45*(12), 6071–6080. <https://doi.org/10.1029/2018gl078210>
- Gray, H. J., Tucker, G. E., Mahan, S. A., McGuire, C., & Rhodes, E. J. (2017). On extracting sediment transport information from measurements of luminescence in river sediment. *Journal of Geophysical Research: Earth Surface*, *122*, 654–677. <https://doi.org/10.1002/2016jf003858>
- Guérin, G., Mercier, N., Nathan, R., Adamiec, G., & Lefrais, Y. (2012). On the use of the infinite matrix assumption and associated concepts: A critical review. *Radiation Measurements*, *47*, 778–785. <https://doi.org/10.1016/j.radmeas.2012.04.004>
- Heyman, J., Stroeven, A. P., Harbor, J. M., & Caffee, M. W. (2011). Too young or too old: Evaluating cosmogenic exposure dating based on an analysis of compiled boulder exposure ages. *Earth and Planetary Science Letters*, *302*(1–2), 71–80. <https://doi.org/10.1016/j.epsl.2010.11.040>
- Hidy, A. J., Gosse, J. C., Pederson, J. L., Mattern, J. P., & Finkel, R. C. (2010). A geologically constrained Monte Carlo approach to modeling exposure ages from profiles of cosmogenic nuclides: An example from Lees Ferry, Arizona. *Geochemistry, Geophysics, Geosystems*, *11*(9), Q0AA10. <https://doi.org/10.1029/2010gc003084>
- Hippe, K. (2017). Constraining processes of landscape change with combined in situ cosmogenic C-14-Be-10 analysis. *Quaternary Science Reviews*, *173*, 1–19. <https://doi.org/10.1016/j.quascirev.2017.07.020>
- Hippe, K., Gordijn, T., Picotti, V., Hajdas, I., Jansen, J. D., Christl, M., et al. (2018). Fluvial dynamics and 14C-10Be disequilibrium on the Bolivian Altiplano. *Earth Surface Processes and Landforms*, *44*(3), 766–780. <https://doi.org/10.1002/esp.4529>
- Huntley, D. J., & Baril, M. R. (1997). The K content of the K-feldspars being measured in optical dating or in thermoluminescence dating. *Ancient TL*, *15*(1), 11–13.
- Huntley, D. J., & Lamothe, M. (2001). Ubiquity of anomalous fading in K-feldspars and the measurement and correction for it in optical dating. *Canadian Journal of Earth Sciences*, *38*(7), 1093–1106. <https://doi.org/10.1139/e01-013>
- Jull, A. J. T., Jull, A., Scott, E. M., & Bierman, P. (2015). The CRONUS-Earth inter-comparison for cosmogenic isotope analysis. *Quaternary Geochronology*, *26*, 3–10. <https://doi.org/10.1016/j.quageo.2013.09.003>
- Kreutzer, S., Schmidt, C., Fuchs, M. C., Dietze, M., Fischer, M., & Fuchs, M. (2012). Introducing an R package for luminescence dating analysis. *Ancient TL*, *30*(1), 1–8.
- Le, K., Lee, J., Owen, L. A., & Finkel, R. (2007). Late Quaternary slip rates along the Sierra Nevada frontal fault zone, California: Slip partitioning across the western margin of the Eastern California Shear Zone–Basin and Range Province. *GSA Bulletin*, *119*(1–2), 240–256. <https://doi.org/10.1130/B25960.1>
- Lewis, C. J., Gardner, J. N., Schultz-Fellenz, E. S., Lavine, A., Reneau, S. L., & Olig, S. (2009). Fault interaction and along-strike variation in throw in the Pajarito fault system, Rio Grande rift, New Mexico. *Geosphere*, *5*(3), 252–269. <https://doi.org/10.1130/GES00198.1>
- Lifton, N. (2016). Implications of two Holocene time-dependent geomagnetic models for cosmogenic nuclide production rate scaling. *Earth and Planetary Science Letters*, *433*, 257–268. <https://doi.org/10.1016/j.epsl.2015.11.006>
- Lifton, N., Goehring, B., Wilson, J., Kubley, T., & Caffee, M. (2015). Progress in automated extraction and purification of in situ C-14 from quartz: Results from the Purdue in situ C-14 laboratory. *Nuclear Instruments and Methods*, *361*, 381–386. <https://doi.org/10.1016/j.nimb.2015.03.028>
- Lifton, N., Sato, T., & Dunai, T. J. (2014). Scaling in situ cosmogenic nuclide production rates using analytical approximations to atmospheric cosmic-ray fluxes. *Earth and Planetary Science Letters*, *386*, 149–160. <https://doi.org/10.1016/j.epsl.2013.10.052>
- Liritzis, I., Stamoulis, K., Papachristodoulou, C., Ioannides, K., Kadereit, A., Zacharias, N., & Li, S.-H. (2013). A re-evaluation of radiation dose-rate conversion factors. *Mediterranean Archaeology and Archaeometry*, *13*, 1–4. [https://doi.org/10.1007/978-3-319-00170-8\\_1](https://doi.org/10.1007/978-3-319-00170-8_1)
- Lukens, C. E., Riebe, C. S., Sklar, L. S., & Shuster, D. L. (2016). Grain size bias in cosmogenic nuclide studies of stream sediment in steep terrain. *Journal of Geophysical Research: Earth Surface*, *121*(5), 978–999. <https://doi.org/10.1002/2016jf003859>
- Malatesta, L. C., Avouac, J.-P., Brown, N. D., Breitenbach, S. F. M., Pan, J., Chevalier, M.-L., et al. (2017). Lag and mixing during sediment transfer across the Tian Shan piedmont caused by climate-driven aggradation-incision cycles. *Basin Research*, *30*(4), 613–635. <https://doi.org/10.1111/bre.12267>
- Matti, J. C., & Morton, D. (1993). Extension and contraction within an evolving divergent strike-slip fault complex: The San Andreas and San Jacinto fault zones at their convergence in Southern California. In R. E. Powell, R. J. Weldon, II, & J. C. Matti (Eds.), *The San Andreas Fault System: Displacement, palinspastic reconstruction, and geologic evolution* (Vol. 178, p 217). Geological Society of America.
- McGuire, C., & Rhodes, E. J. (2015). Downstream MET-IRSL single-grain distributions in the Mojave River, Southern California: Testing assumptions of a virtual velocity model. *Quaternary Geochronology*, *30*, 239–244. <https://doi.org/10.1016/j.quageo.2015.02.004>
- Nichols, K. A., & Goehring, B. M. (2019). Isolation of quartz for cosmogenic in situ <sup>14</sup>C analysis. *Geochronology*, *1*(1), 43–52. <https://doi.org/10.5194/gchron-1-43-2019>
- Nishiizumi, K., Imamura, M., Caffee, M. W., Southon, J. R., Finkel, R. C., & McAninch, J. (2007). Absolute calibration of <sup>10</sup>Be AMS standards. *Nuclear Instruments and Methods*, *258*, 403–413. <https://doi.org/10.1016/j.nimb.2007.01.297>
- Owen, L. A., Clemmens, S. J., Finkel, R. C., & Gray, H. (2014). Late Quaternary alluvial fans at the eastern end of the San Bernardino Mountains, Southern California. *Quaternary Science Reviews*, *87*, 114–134. <https://doi.org/10.1016/j.quascirev.2014.01.003>
- Owen, L. A., Davis, T., Caffee, M. W., Budinger, F., & Nash, D. (2011). Surface ages and rates of erosion at the Calico Archaeological Site in the Mojave Desert, Southern California. *Geomorphology*, *125*(1), 40–50. <https://doi.org/10.1016/j.geomorph.2010.08.013>

- Pigati, J. S., Lifton, N. A., Jull, A. J. T., & Quade, J. (2010). A simplified in situ cosmogenic  $^{14}\text{C}$  extraction system. *Radiocarbon*, *52*(3), 1236–1243. [https://doi.org/10.2458/azu\\_js\\_rc.v52i3.362210.1017/s0033822200046324](https://doi.org/10.2458/azu_js_rc.v52i3.362210.1017/s0033822200046324)
- Powell, R. E. (1993). Balanced palinspastic reconstruction of pre-late Cenozoic paleogeology, Southern California: Geologic and kinematic. In R. E. Powell, R. J. Weldon II, & J. C. Matti (Eds.), *The San Andreas Fault System: Displacement, palinspastic reconstruction, and geologic evolution*, (Vol. 178, pp. 1–106). Geological Society of America. <https://doi.org/10.1130/mem178-p1>
- Prush, V. B., & Oskin, M. E. (2020). A mechanistic erosion model for cosmogenic nuclide inheritance in single-clast exposure ages. *Earth and Planetary Science Letters*, *535*, 116066. <https://doi.org/10.1016/j.epsl.2020.116066>
- Remeika, P., & Lindsay, L. (1992). *Geology of Anza-Borrego: Edge of creation*. Sunbelt Publications.
- Rhodes, E. J. (2015). Dating sediments using potassium feldspar single-grain IRSL: Initial methodological considerations. *Quaternary International*, *362*, 14–22. <https://doi.org/10.1016/j.quaint.2014.12.012>
- Rittenour, T. M. (2008). Luminescence dating of fluvial deposits: Applications to geomorphic, paleoseismic and archaeological research. *Boreas*, *37*, 613–635. <https://doi.org/10.1111/j.1502-3885.2008.00056.x>
- Ritter, J. B., Miller, J. R., Enzel, Y., & Wells, S. G. (1995). Reconciling the roles of tectonism and climate in Quaternary alluvial fan evolution. *Geology*, *23*(3), 245–248. [10.1130/0091-7613\(1995\)023<0245:rtrota>2.3.co;2](https://doi.org/10.1130/0091-7613(1995)023<0245:rtrota>2.3.co;2)
- Saha, S., Moon, S., Brown, N. D., Rhodes, E. J., Scharer, K. M., McPhillips, D., et al. (2021). Holocene depositional history inferred from single-grain luminescence ages in Southern California, North America. *Geophysical Research Letters*, *48*(15), e2021GL092774. <https://doi.org/10.1029/2021gl092774>
- Salisbury, J. B., Arrowsmith, J. R., Brown, N., Rockwell, T., Akciz, S., & Ludwig, L. G. (2018). The age and origin of small offsets at Van Matre Ranch along the San Andreas Fault in the Carrizo Plain, California. *Bulletin of the Seismological Society of America*, *108*(2), 639–653. <https://doi.org/10.1785/0120170162>
- Scheuwly-Bollschweiler, M., Stoffel, M., & Rudolf-Miklau, F. (Eds.). (2013). *Dating torrential processes on fans and cones. Methods and their application for hazard and risk assessment* (p. 439). Springer. <https://doi.org/10.1007/978-94-007-4336-6>
- Stockmeyer, J. M., Shaw, J. H., Brown, N. D., Rhodes, E. J., Richardson, P. W., Wang, M., et al. (2017). Active thrust sheet deformation over multiple rupture cycles: A quantitative basis for relating terrace folds to fault slip rates. *GSA Bulletin*, *129*(9–10), 1337–1356. <https://doi.org/10.1130/b31590.1>
- Thomsen, K. J., Murray, A. S., Jain, M., & Bøtter-Jensen, L. (2008). Laboratory fading rates of various luminescence signals from feldspar-rich sediment extracts. *Radiation Measurements*, *43*(9–10), 1474–1486. <https://doi.org/10.1016/j.radmeas.2008.06.002>